Spectral relationships for atmospheric correction. II. Improving NASA's standard and MUMM near infra-red modeling schemes.

C. Goyens,[1] **C. Jamet,**[1*] **and K. G. Ruddick**[2]

[1] *CNRS, UMR 8187, Université Lille Nord de France, ULCO, LOG, F-62930 Wimereux, France*

[2] *Management Unit of the North Sea Mathematical Models (MUMM), Royal Belgian Institute for Natural Sciences (RBINS), 100 Gulledelle, B-1200 Brussels, Belgium*

[*] *cedric.jamet@univ-littoral.fr*

Abstract: Spectral relationships, reflecting the spectral dependence of water-leaving reflectance, $\rho_w(\lambda)$, can be easily implemented in current AC algorithms with the aim to improve $\rho_w(\lambda)$ retrievals where the algorithms fail. The present study evaluates the potential of spectral relationships to improve the MUMM (Ruddick et al., 2006, Limnol. Oceanogr. **51**, 1167-1179) and standard NASA (Bailey et al., 2010, Opt. Express **18**, 7521-7527) near infra-red (NIR) modeling schemes included in the AC algorithm to account for non-zero $\rho_w(\lambda_{NIR})$, based on *in situ* coastal $\rho_w(\lambda)$ and simulated Rayleigh corrected reflectance data. Two modified NIR-modeling schemes are investigated: (1) the standard NASA NIR-modeling scheme is forced with bounding relationships in the red spectral domain and with a NIR polynomial relationship and, (2) the constant NIR $\rho_w(\lambda)$ ratio used in the MUMM NIR-modeling scheme is replaced by a NIR polynomial spectral relationship. Results suggest that the standard NASA NIR-modeling scheme performs better for all turbidity ranges and in particular in the blue spectral domain (percentage bias decreased by approximately 50%) when it is forced with the red and NIR spectral relationships. However, with these new constrains, more reflectance spectra are flagged due to non-physical Chlorophyll-a concentration estimations. The new polynomial-based MUMM NIR-modeling scheme yielded lower $\rho_w(\lambda)$ retrieval errors and particularly in extremely turbid waters. However, including the polynomial NIR relationship significantly increased the sensitivity of the algorithm to errors on the selected aerosol model from nearby clear water pixels.

OCIS codes: (010.0010) Atmospheric and oceanic optics; (010.1285) Atmospheric correction; (010.4450) Oceanic optics; (010.1690) Color.

References and links

1. H. R. Gordon and M. Wang, "Retrieval of water-leaving radiance and aerosol optical thickness over the oceans with SeaWiFS: A preminilary algorithm," Appl. Opt. **33**, 443-452 (1994).
2. D. A. Siegel, M. Wang, S. Maritorena, and W. Robinson, "Atmospheric correction of satellite ocean color imagery: The black pixel assumption," Appl. Opt. **39**, 3582-3591 (2000).

#193504 - $15.00 USD Received 8 Jul 2013; revised 12 Aug 2013; accepted 13 Aug 2013; published 3 Sep 2013

3. R. P. Stumpf, R. A. Arnone, J. R. W. Gould, P. M. Martinolich, and, V. Ransibrahmanakul, "A partially coupled ocean-atmosphere model for retrieval of water-leaving radiance from SeaWiFS in coastal waters," in *SeaWiFS Postlaunch Technical Report Series, Volume 22, NASA Tech. Memo. 2003-206892*, S. B. Hooker and E. R. Firestone, eds., (NASA Goddard Space Flight Center, Greenbelt, Maryland), pp. 51-59 (2003).
4. K. G. Ruddick, V. De Cauwer, Y. Park and G. Moore, "Seaborne measurements of near infrared water-leaving reflectance: The similarity spectrum for turbid waters," Limnol. Oceanogr. **51**, 1167-1179 (2006).
5. S. W. Bailey, B. A. Franz, and P. J. Werdell, " Estimations of near-infrared water-leaving reflectance for satellite ocean color data processing," Opt. Express **18**, 7521-7527 (2010).
6. K. G. Ruddick, F. Ovidio, and M. Rijkeboer, "Atmospheric correction of SeaWiFS imagery for turbid coastal and inland waters," Appl. Opt. **39**, 897-912 (2000).
7. C. Jamet, H. Loisel, C. P. Kuchinke, K. Ruddick, G. Zibordi, and H. Feng, "Comparison of three SeaWiFS atmospheric correction algorithms for turbid waters using AERONET-OC measurements," Remote Sens. Environ. **115**(8), 1955-1965 (2011).
8. C. Goyens, C. Jamet, and T. Schroeder, " Evaluation of four atmospheric correction algorithms for MODIS-Aqua images over contrasted coastal waters," Remote Sens. Environ. **131**, 63-75 (2013).
9. T. Schroeder, I. Behnert, M. Schaale, J. Fischer, and R. Doerffer, " Atmospheric correction algorithm for MERIS above case-2 waters, " Int. J. Remote Sens. **28**(7), 1469-1486 (2007).
10. M. Wang, S. Son, and W. Shi, " Evaluation of MODIS SWIR and NIR-SWIR atmospheric correction algorithms using SeaBASS data, " Remote Sens. Environ. **113**, 635-644 (2009).
11. M. Doron, S. Bélanger, D. Doxaran, and M. Babin, "Spectral variations in the near-infrared ocean reflectance," Remote Sens. Environ. **115**, 1617-1631 (2011).
12. C. Goyens, C. Jamet, and K. Ruddick, " Spectral relationships for atmospheric correction. I. Review and evaluation of red and near infra-red spectral relationships, " accepted for publication in Opt. Express (2013).
13. R. C. Smith and W. H. Wilson, "Ship and satellite bio-optical research in the Calofornia Bight," in *Oceanography from Space*, J. F. R. Gower, eds., (Plenum Publishing Corporation, New York), pp. 281-294 (1980).
14. R. W. Austin and T. Petzold, "The determination of the diffuse attenuation coefficient of sea water using the Coastal Zone Color Scanner," in *Oceanography from Space*, J. F. R. Gower, eds., (Plenum Publishing Corporation, New York), pp. 239-256 (1980).
15. A. Bricaud and A. Morel,"Atmospheric corrections and interpretation of marine radiances in CZCS imagery: Use of a reflectance model," Oceanol. Acta **33-50 N.SP**, (1987).
16. B. Sturm, V. Barale, D. Larkin, J. H. Andersen, and M. Turner, " OCEAN code: the complete set of algorithms and models for the level 2 processing of European CZCS historical data, " Int. J. Remote Sens. **20**(7), 1219-1248 (1999).
17. J. Ahn, Y. Park, J. Ryu, B. Lee, and I. S. Oh, "Development of Atmospheric Correction Algorithm for Geostationary Ocean Color Imager (GOCI)," Ocean Sci. J. **47**(3), 247-259 (2012).
18. M. Wang, W. Shi and L. Jiang, " Atmospheric correction using near-infrared bands for satellite ocean color data processing in the turbid western pacific region," Opt. Express **20**, 741-753 (2012).
19. Z. Lee, B. Lubac, J. Werdell, and, R. Arnone, "An update of the Quasi-Analytical Algorithm (QAA v5), " available at: `http://www.ioccg.org/groups/Software_OCA/QAA_v5.pdf` (2009).
20. E. P. Shettle and R. W. Fenn, "Models of the aerosols of the lower atmosphere and the effects of humidity variations on their optical properties, " Rep. AFGL-TR-79-0214, U.S. Air Force Geophysics Laboratory, Hanscom Air Force Base, Mass. (1979).
21. J. E. O'Reilly, S. Maritorena, D. Siegel, M. C. O'Brien, D. Toole, B. G. Mitchell, M. Kahru, F. P. Chavez, P. Strutton, G. E. Cota, S. B. Hooker, C. R. McClain, K. L. Carder, F. Muller-Krager, L. Harding, A. Magnuson, D. Phinney, G. F. Moore, J. Aiken, K. R. Arrigo, R. Letelier, and M. Culver, " Ocean color chlorophyll a algorithms for SeaWiFS, OC2, and OC4: Version 4, " in *SeaWiFS Postlaunch Technical Report Series, Volume 11, NASA Tech. Memo. 2000-206892*, S. B. Hooker and E. R. Firestone, eds., (NASA Goddard Space Flight Center, Greenbelt, Maryland), pp. 9-23 (2000).
22. P. J. Werdell and S. W. Bailey, " An improved bio-optical data set for ocean color algorithm development and satellite data product validation," Remote Sens. Environ. **98**, 122-140 (2005).
23. Z. P. Lee, K. L. Carder, C. D. Mobley, R. G. Steward, and J. S. Patch, " Hyperspectral remote sensing for shallow waters: 1. A semianalytical model, " Appl. Opt. **37**(27) 6329-6338 (1998).
24. Z. Lee, K. L. Carder, and R. A. Arnone, " Deriving inherent optical properties from water color: a multiband quasi-analytical algorithm for optically deep waters, " Appl. Opt. **41**(27), 5755-5772 (2002).
25. A. Morel and L. Prieur, "Analysis of variations in ocean color, " Limnol. Oceanogr. **22**, 709-722 (1977).

1. Introduction

The marine reflectance $\rho_w(\lambda)$ estimated from ocean color satellite images is directly related to the inherent optical properties of the water (e.g., sea water absorption $a(\lambda)$ and backscattering $b_b(\lambda)$) allowing the derivation of biogeochemical parameters over the oceans. The accuracy of

#193504 - $15.00 USD Received 8 Jul 2013; revised 12 Aug 2013; accepted 13 Aug 2013; published 3 Sep 2013

these satellite derived parameters depends however on the processing of the sensor-measured radiance at the top of the atmosphere (TOA) used to obtain $\rho_w(\lambda)$. This processing includes, among others, the removal of the atmospheric contribution, the so-called atmospheric correction (AC) [1].

Initially, it was assumed that sea water absorbs all the incident light in the NIR spectral region (referred to as the black pixel assumption) allowing to estimate the atmospheric contributions and to select the appropriate aerosol model from the total signal. Next, the aerosol properties are extrapolated from the NIR to the visible spectral domain to obtain $\rho_w(\lambda)$ [1] (referred to as the GW94 AC algorithm). However in highly productive or turbid waters the assumption of zero NIR $\rho_w(\lambda)$ is not valid [2, 3]. Assuming zero $\rho_w(\lambda_{NIR})$ generally leads to an overestimation of the aerosol contributions and subsequently to an underestimation of $\rho_w(\lambda)$ in highly productive or turbid waters [2]. Numerous algorithms have been developed with alternative hypotheses or including NIR-modeling schemes to account for the NIR ocean contribution to the measured signal [2–6]. However, global evaluations of these algorithms concluded that improvement is still required, especially in optically complex waters [7, 8].

In a previous study, Goyens et al. [8] concluded, based on a validation of MODIS-Aqua images processed with four commonly used AC algorithms [4, 5, 9, 10], that the standard NASA GW94-based AC algorithm, which includes a NIR-modeling scheme to retrieve $\rho_w(\lambda_{NIR})$ [3, 5] (hereafter referred to as the STD algorithm), provided overall the best performances. However, in water masses optically dominated by detrital and mineral material, the GW94-based AC algorithm assuming a NIR similarity spectrum to account for non-zero $\rho_w(\lambda_{NIR})$, [4, 6] (hereafter referred to as the MUMM algorithm) performed slightly better. The NIR-modeling scheme used in the STD algorithm is based on an iterative procedure including a bio-optical model with a Chlorophyll-a (Chl_a) based relationship to estimate $a(667)$ and assumptions on $b_b(\lambda)$ to extrapolate $\rho_w(\lambda)$ from the red to the NIR spectral domain [5]. In the MUMM algorithm, the GW94 AC algorithm is extended to turbid waters by considering spatial homogeneity in the aerosol properties over the area of interest and approximating the NIR $\rho_w(\lambda)$ ratio by a universal constant [4, 6]. However, these assumptions show some limitations leading to imperfections in the AC. For instance, in waters optically dominated by non-algal particles, the Chl_a based relationship used in the bio-optical model of the STD algorithm may not be appropriate resulting in imperfections in the retrieved backscattering coefficients and subsequently in $\rho_w(\lambda_{NIR})$. Similarly, the constant NIR reflectance ratio used in the MUMM algorithm relies on the assumption that the NIR reflectance spectral shape is merely determined by the pure water absorption [4, 6]. However, this assumption is not verified for all turbidity ranges and is valid for a limited spectral range [4, 11, 12].

An alternative to improve the STD algorithm is to constrain the iterative NIR-modeling scheme with spectral relationships. Similarly, a NIR spectral relationship may be used to correct the MUMM algorithm when the constant NIR reflectance ratio is not valid. Similar approaches have already been applied in several studies [12–18]. However, as observed by Goyens et al. [12], most spectral relationships appeared to be only valid for a certain range of turbidity. Nonetheless, the authors concluded that the bounding red spectral relationships, suggested by Lee et al. [19] to correct $\rho_w(667)$ according to $\rho_w(555)$ in the Quasi-Analytical Algorithm, and that the NIR polynomial relationship, suggested by Wang et al. [18] to extent the GW94 AC algorithm to the turbid western Pacific region for the processing of the GOCI ocean color images, were globally valid and potentially useful to improve satellite $\rho_w(\lambda)$ retrievals.

The objective of this study is to evaluate if the STD and MUMM algorithms can be improved by forcing the NIR-modeling schemes in both algorithms with these spectral relationships. Two modified NIR-modeling schemes are evaluated: (1) a modified MUMM NIR modeling scheme where the NIR constant $\rho_w(\lambda)$ ratio is replaced by the polynomial NIR spectral relationship,

#193504 - $15.00 USD Received 8 Jul 2013; revised 12 Aug 2013; accepted 13 Aug 2013; published 3 Sep 2013

and (2) a modified STD NIR-modeling scheme constrained with the bounding red spectral relationships suggested by Lee et al. [19] and the NIR polynomial relationship [18] to evaluate $\rho_w(869)$ from $\rho_w(748)$. Hence two original algorithms are taken into account (i.e., MUMM and STD algorithms) and different modifications are applied to each algorithm.

The evaluation is based on a sensitivity test including *in situ* $\rho_w(\lambda)$ spectra from European and Southern Atlantic coastal waters. Data and methods are outlined in section 2. To evaluate the degree of improvement, initial algorithms are compared with modified algorithms, briefly discussed in sections 2.2 and 2.3, respectively. The performances of the initial algorithms are evaluated for moderately and very turbid waters (section 3.1) and compared to the modified algorithms evaluated and discussed in section 3.2.

2. Data and methods

2.1. Sensitivity study set-up

The top of atmosphere (TOA) reflectance, $\rho^{TOA}(\lambda)$, is derived from the sensor-measured radiance and corrected for gas absorption, Rayleigh scattering, white-caps reflection and sun glint, to obtain the Rayleigh corrected reflectance, $\rho_{rc}^{TOA}(\lambda)$, written as [1]:

$$\rho_{rc}^{TOA} = \rho_a^{TOA}(\lambda) + \rho_{ra}^{TOA}(\lambda) + t_{\theta_v}(\lambda)t_{\theta_0}(\lambda)\rho_w(\lambda). \tag{1}$$

where $\rho_a^{TOA}(\lambda)$ and $\rho_{ra}^{TOA}(\lambda)$ represent the scattered sunlight by the aerosols and the coupling between both air and aerosol molecules, respectively. $t_{\theta_v}(\lambda)$ is the diffuse transmittance of the atmosphere along the viewing direction and $t_{\theta_0}(\lambda)$ is the diffuse transmittance of the atmosphere along the incident direction. According to Eq. (1), if the optical properties and the concentrations of the aerosols are known, the quantities $\rho_a^{TOA}(\lambda)$, $\rho_{ra}^{TOA}(\lambda)$, $t_{\theta_0}(\lambda)$ and $t_{\theta_v}(\lambda)$ can be estimated and subsequently the above water $\rho_w(\lambda)$. For notational simplicity, the TOA notation is dropped hereafter.

For the present research a simulated dataset of $\rho_{rc}(\lambda)$ is build by combining the 105 *in situ* $\rho_w(\lambda)$ spectra (from above water TRIOS Ramses hyper-spectral radiometers, further detailed in the companion paper of this study [12]) with a simplified power law model for the multiple-scattering aerosol reflectance, $\rho_{am}(\lambda_0)$ (the sum of $\rho_a(\lambda_0)$ and $\rho_{ra}(\lambda_0)$ in Eq. (1)):

$$\rho_{am}(\lambda) = \rho_{am}(\lambda_0)\left(\frac{\lambda}{\lambda_0}\right)^{-\eta} \tag{2}$$

with η being the Ångström coefficient for the aerosol reflectance. For these tests we set the atmospheric diffuse transmittances, $t_{\theta_v}(\lambda)$ and $t_{\theta_0}(\lambda)$, to 1 and simulate $\rho_{rc}(\lambda)$ simply as the sum of $\rho_{am}(\lambda)$ and the *in situ* $\rho_w(\lambda)$. As shown by the flowchart in Fig. 1, $\rho_{rc}(\lambda)$ is then inverted using either the STD or the MUMM algorithm to estimate $\rho_w(\lambda)$ which for a perfect model would be equal to the *in situ* $\rho_w(\lambda)$.

For the sensitivity study two coastal models are selected, considered as the dominating aerosol types in coastal regions and derived from the work of Shettle and Fenn [20] and introduced by Gordon and Wang [1] with 50 and 90% relative humidity (hereafter referred to as C50 and C90). The corresponding Ångström coefficients η are set equal to 0.75 and 0.43, respectively, and $\rho_{am}(\lambda_0)$ at 869 nm to 0.015.

The initial and modified algorithms are evaluated and compared based on the median percentage bias between the estimated and *in situ* $\rho_w(\lambda)$ ($\rho_w^{est}(\lambda)$ and $\rho_w^{in\ situ}(\lambda)$, respectively):

$$\text{Bias} = 100\ \frac{\rho_w^{est}(\lambda) - \rho_w^{in\ situ}(\lambda)}{\rho_w^{in\ situ}(\lambda)} \tag{3}$$

#193504 - $15.00 USD Received 8 Jul 2013; revised 12 Aug 2013; accepted 13 Aug 2013; published 3 Sep 2013

A distinction is also made between moderately and very turbid waters defined as the spectra presenting $\rho_w(869)$ values between 10^{-4} and 3.10^{-3} and superior to 3.10^{-3}, respectively. All spectra presented $\rho_w(\lambda_{NIR})$ values above 10^{-4}, which is approximately the upper limit for which the GW94 AC algorithm can be successfully applied [2]. Out of the 105 spectra, 53% present moderate turbidity with $\rho_w(869)$ ranging from 10^{-4} to 3.10^{-3} and 47% of the data present very turbid waters with $\rho_w(869)$ exceeding 3.10^{-3}. This latter value corresponds to the threshold used by Wang et al. [10] to switch for the SWIR algorithm in the combined NIR-SWIR GW94-based AC process. Among the very turbid waters, extremely turbid waters are also investigated. These are water masses presenting $\rho_w(869)$ values superior to 10^{-2} and represent about 23% of the total *in situ* dataset.

2.2. Initial STD and MUMM algorithms

2.2.1. The STD algorithm

The NIR-modeling scheme within the STD algorithm, initially developed by Stumpf et al. [3] and later revised by Bailey et al. [5], uses an iterative method including a bio-optical model to account for the water contribution in the NIR region of the spectrum. The STD algorithm can be resumed as follows: First the algorithm uses the GW94 AC algorithm, assuming the black pixel assumption, to obtain a first guess in $\rho_w(\lambda)$. Blue and green $\rho_w(\lambda)$ estimations are then used to estimate Chl_a concentrations (MODIS Chl-a OC3 algorithm [21], assumption 1 in Fig. 1), which in turn serves to retrieve particulate and CDOM absorption in the red [22] (assumption 2 in Fig. 1), $a_{pg}(667)$. Knowing $a_{pg}(\lambda_{red})$ and below water $\rho_w^-(\lambda_{red})$ (by converting the estimated above water $\rho_w(667)$ to below water radiance reflectance [23]) it is possible to determine the red particulate backscattering coefficient, $b_{bp}(\lambda_{red})$. Next, $b_{bp}(\lambda_{NIR})$ is approximated by a power-law function of wavelength [24] (assumption 3 in Fig. 1). As, in the NIR region of the spectrum, absorption by CDOM, phytoplankton-related pigments, and other suspended particulate matter is assumed to be negligible, $a(\lambda_{NIR})$ can be approximated by the pure water absorption $a_w(\lambda_{NIR})$. Accordingly, knowing $a(\lambda_{NIR})$ and $b_{bp}(\lambda_{NIR})$, below water $\rho_w^-(\lambda_{NIR})$ can be estimated [25] and converted in above water $\rho_w(\lambda_{NIR})$. $\rho_w(\lambda_{NIR})$ is removed from $\rho_{rc}(\lambda_{NIR})$ and the newly estimated $\rho_{rc}(\lambda)$ is then inverted again with the GW94 AC algorithm to obtain $\rho_w(\lambda)$.

The process is re-iterated until $\rho_w(\lambda_{red})$ converges or if the maximum number of iterations is exceeded. In this study, when the estimated Chl_a is non-physical (e.g., because the retrieved $\rho_w(\lambda)$ are negative) or if the estimated $\rho_{am}(\lambda_0)$ is negative, an AC failure flag is assigned to the spectrum and $\rho_{am}(\lambda_0)$ is set to 0 and Chl_a to 10 mg l^{-1} for the next iteration. If the AC failure flag is assigned twice to a same spectrum, it is excluded for further data analysis.

2.2.2. The MUMM algorithm

The MUMM algorithm includes two alternative assumptions, one on the atmosphere (assumption 1 in Fig. 1) and one on the water optical properties, the NIR similarity spectrum assumption (assumption 2 in Fig. 1) [4,6]. The first assumption is based on the fact that the atmosphere composition does not vary significantly in space and time and therefore the Ångström coefficient for the aerosol reflectance, η, can be considered as spatially homogeneous over the area of interest. In clear waters, where $\rho_w(\lambda)$ in the NIR region of the spectrum is close to zero, $\rho_a(\lambda)+\rho_{ra}(\lambda)$ can be approximated by $\rho_{rc}(\lambda)$ and, subsequently, η can be retrieved. The clear water retrieved η is then used for the AC of the entire image.

The second assumption arises from the fact that the sea-water spectrum shape in the NIR spectral domain is largely determined by pure water absorption, and hence invariant. The magnitude of the signal is approximately proportional to the backscatter coefficient. Consequently, the ratio of any two NIR water leaving reflectances, $\alpha(\lambda_i,\lambda_j)$, is constant. For MODIS-Aqua

#193504 - $15.00 USD Received 8 Jul 2013; revised 12 Aug 2013; accepted 13 Aug 2013; published 3 Sep 2013

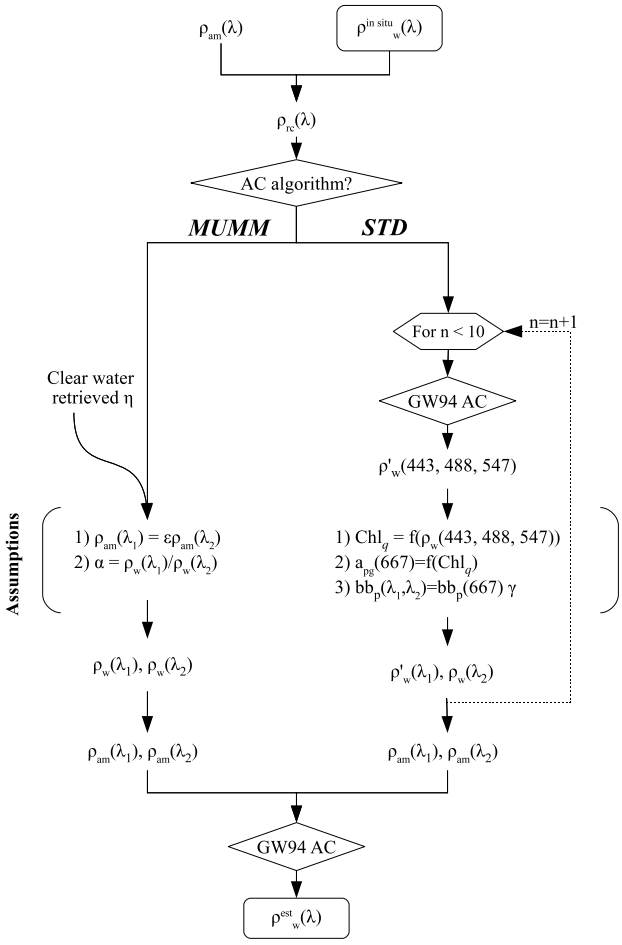

Fig. 1. Schematic flowchart of the sensitivity study set-up for the STD and MUMM algorithms. $\rho_w^{in\ situ}(\lambda)$ and $\rho_w^{est}(\lambda)$ are the *in situ* and estimated $\rho_w(\lambda)$, respectively, and λ_1 and λ_2 designate the two wavelengths in the NIR spectral region. Dashed lines indicate the iterative processes for the STD algorithm.

#193504 - $15.00 USD Received 8 Jul 2013; revised 12 Aug 2013; accepted 13 Aug 2013; published 3 Sep 2013

images $\alpha(748,869)$ is defined as:

$$\alpha = \frac{\rho_w(748)}{\rho_w(869)} = 1.945 \tag{4}$$

Next, knowing η and $\alpha(\lambda_i,\lambda_j)$, $\rho_{am}(\lambda)$ is estimated for two NIR bands allowing to retrieve the appropriate aerosol model.

$$\rho_{am}(\lambda_i) = \varepsilon(\lambda_i,\lambda_j)\frac{\alpha(\lambda_i,\lambda_j)\rho_{rc}(\lambda_j) - \rho_{rc}(\lambda_i)}{\alpha(\lambda_i,\lambda_j) - \varepsilon(\lambda_i,\lambda_j)} \tag{5}$$

$$\rho_{am}(\lambda_j) = \frac{\alpha(\lambda_i,\lambda_j)\rho_{rc}(\lambda_j) - \rho_{rc}(\lambda_i)}{\alpha(\lambda_i,\lambda_j) - \varepsilon(\lambda_i,\lambda_j)} \tag{6}$$

The initial GW94 AC algorithm is then run again but forced with the previously selected aerosol model.

As shown in Fig. 1, the MUMM algorithm requires thus an a priori defined η. For the sensitivity study, a correct retrieved η is initially assumed. Next, to assess the sensitivity of the algorithm to errors on the selected aerosol model, we consider an η value corresponding to the C90 aerosol model while the C50 aerosol model was used to simulate $\rho_{rc}(\lambda)$ (error on η of $\sim -40\%$) and vice versa (error on η of $\sim 70\%$).

2.3. Modified STD and MUMM algorithms

2.3.1. Polynomial-based MUMM algorithm

The MUMM algorithm is modified here to take into account also extremely turbid waters. Indeed, the validation exercise conducted by Goyens et al. [12] showed that the validity range of the constant NIR reflectance ratio [4, 6] was limited to moderately and very turbid waters with $\rho_w(\lambda_{NIR}) < 10^{-2}$, while the polynomial function of Wang et al. [18] was also valid for extremely turbid waters. Subsequently, in order to improve $\rho_w(\lambda)$ retrievals in extremely turbid waters, the NIR constant reflectance ratio in the MUMM algorithm (assumption 2 in Fig. 1) is replaced by the polynomial function of Wang et al. [18] (therefore referred to as the polynomial-based MUMM algorithm). This includes some modifications in the initial algorithm. Using Eq. (1) and the polynomial function from Wang et al. [18], the following relationships and unknown quantities are obtained:

$$\rho_{rc}(748) = \rho_{am}(748) + t^*_{748}\rho_w(748) \tag{7}$$

$$\rho_{rc}(869) = \rho_{am}(869) + t^*_{869}\left[a\rho_w(748) + b\rho_w(748)^2\right] \tag{8}$$

where a and b are the constant values of the polynomial function [18] and t^*_λ the viewing and incident atmospheric transmittance corrected for the two-way ozone and oxygen absorption using the terminology of Ruddick et al. [4].

Provided that the aerosol model is correctly retrieved, the atmospheric correction parameter $\varepsilon(748,869)$ (written hereafter as ε for notational simplicity) is equal to the aerosol reflectance ratio at 748 and 869 nm and thus, according to Eq. (2), related to η as follow:

$$\varepsilon = \frac{\rho_{am}(748)}{\rho_{am}(869)} = \left(\frac{\lambda}{\lambda_0}\right)^{-\eta} \tag{9}$$

Eq. (8) can then be rewritten as:

$$\rho_{rc}(869) = \frac{1}{\varepsilon}\rho_{am}(748) + at^*_{869}\rho_w(748) + bt^*_{869}\rho_w(748)^2. \tag{10}$$

#193504 - $15.00 USD Received 8 Jul 2013; revised 12 Aug 2013; accepted 13 Aug 2013; published 3 Sep 2013

Accordingly, the system Eq.(7)-ε Eq.(10) gives:

$$b\varepsilon t^*_{869}\rho_w(748)^2 + [a\varepsilon t^*_{869} - t^*_{748}]\,\rho_w(748) + [\rho_{rc}(748) - \varepsilon\rho_{rc}(869)] = 0. \quad (11)$$

$\rho_{rc}(\lambda)$ at 748 and 869 nm are known for each spectra and t^*_λ is derived from the viewing and incident geometry and selected aerosol model. Hence, the remaining unknown quantity is $\rho_w(748)$. Eq. (11) is a quadratic function with two solutions, one of which is clearly non-physical. Accordingly, the unique solution for $\rho_w(748)$ is:

$$\rho_w(748) = \frac{[t^*_{748} - a\varepsilon t^*_{869}] - \sqrt{[a\varepsilon t^*_{869} - t^*_{748}]^2 - 4b\varepsilon t^*_{869}[\rho_{rc}(748) - \varepsilon\rho_{rc}(869)]}}{2b\varepsilon t^*_{869}} \quad (12)$$

Next, knowing $\rho_w(748)$, $\rho_w(869)$ can be retrieved by evaluating the polynomial function of Wang et al. [18] and, by means of Eqs. (1) and (2), $\rho_w(\lambda)$ can be retrieved for the entire spectrum.

2.3.2. Constrained STD algorithm

To improve $\rho_w(\lambda)$ retrievals, red and NIR spectral relationships are used to constrain the NIR-modeling scheme within the STD algorithm (therefore referred to as the constrained-STD algorithm). The red spectral relationships are already used as bounding relationships in the last updated version of the Quasi Analytical Algorithm (QAA v5) to correct imperfections in the retrieved $\rho_w(667)$ [19]. Similarly to the polynomial relationship suggested by Wang et al. [18], these red spectral relationships have been validated previously by Goyens et al. [12] with the *in situ* data mentioned in section 2.1. To force the STD algorithm, the spectral relationships are implemented within the iterative process as follows: If within the iterative process, the previously retrieved $\rho_w(555)$ is non-negative and $\rho_w(667)$ is out of limit according the bounding red spectral relationships, $\rho_w(667)$ is corrected and set equal to the closest limit. Next, the NIR spectral polynomial relationship [18] is used to retrieve $\rho_w(869)$ from the estimated $\rho_w(748)$, avoiding imperfections due to the extrapolation of $b_{bp}(\lambda)$ from 667 to 869 nm.

3. Results and discussion

3.1. Performances of initial STD and MUMM algorithms in turbid waters

To delineate the areas of improvements, the performances of the initial AC algorithms are first evaluated. Statistics (median, first and third quartile) of the percentage bias between *in situ* and estimated $\rho_w(\lambda)$ for the STD and MUMM algorithms are shown in Fig. 2, for moderately and very turbid waters and when considering only extremely turbid waters. Relative performances of the algorithms are similar when the C50 or C90 aerosol model is considered and the percentage bias calculated with the C50 aerosol model and the C90 aerosol model remain close. Therefore, results are shown here with the C50 aerosol model only.

For moderately turbid waters, the two algorithms retrieves the same number of reflectance spectra. In contrast, due to AC failure (observed for 9 spectra) and because $\rho_w(667)$ did not converged after 10 iterations (for 1 spectrum), for very turbid waters the STD algorithm retrieves 46 reflectance spectra out of the 56. The excluded spectra present all $\rho_w(869)$ values superior to 10^{-2} (defined previously as extremely turbid).

The STD algorithm tends to underestimate $\rho_w(\lambda)$ at all wavelengths for moderately turbid waters (median bias ranging from -51% to -3%) [Figs. 2(a)-2(e)]. For the very turbid waters the algorithm provides relatively good results in the green but underestimates $\rho_w(\lambda)$ in the blue and largely overestimates $\rho_w(\lambda)$ at 869 nm (median bias of -13% and 22%, respectively) [Figs.

#193504 - $15.00 USD Received 8 Jul 2013; revised 12 Aug 2013; accepted 13 Aug 2013; published 3 Sep 2013

2(a)-2(e)]. When considering only the most turbid waters ($\rho_w(869) > 10^{-2}$, 14 extremely turbid spectra), the underestimation of $\rho_w(\lambda)$ in the blue spectral domain is even more pronounced with a median bias ranging from -60% at 412 nm to 18% at 869 nm. This suggests that the STD NIR-modeling scheme is appropriate for very turbid waters, however negative $\rho_w(\lambda)$ values in the blue are still retrieved and the performance of the algorithm decreases with an increase in turbidity. For moderately turbid waters, the assumptions made in the STD algorithm results in relatively low errors at 412 nm but in large retrieval errors in the red and NIR spectral domain.

For moderately turbid waters and over the 412-667 nm spectral range, the median percentage bias varies from -2% to -8% for the MUMM algorithm. However, at 748 and 869 nm, the median percentage bias reaches values up to -30 and -41%, respectively [Figs. 2(f)-2(j)]. For very turbid waters, the median bias ranges from -0.5% to -5% [Figs. 2(f)-2(j)]. When considering only the most turbid waters ($\rho_w(869) > 10^{-2}$, 24 extremely turbid spectra) the median bias further decreases ranging from -18% to -4%. This may be explained by the underestimation of the water signal in extremely turbid waters when a constant NIR reflectance ratio is considered. Indeed, as observed with the validation exercise of Doron et al. [11] and Goyens et al. [12], the constant NIR reflectance ratio used in the MUMM algorithm tends to underestimate $\rho_w(\lambda)$ in the NIR spectral domain when $\rho_w(\lambda_{NIR})$ increases. Note however that these results are obtained when η is correctly estimated over the clear water pixels and thus considering that the assumption of spatial homogeneity in aerosol properties is verified.

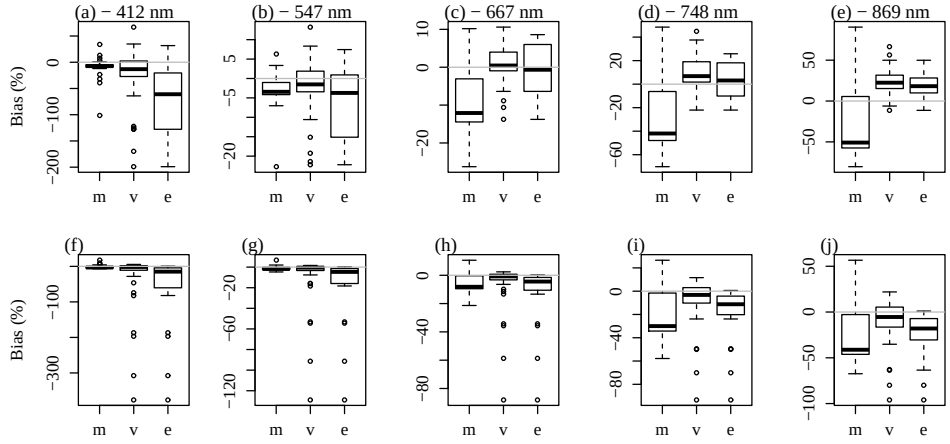

Fig. 2. Box plots of percentage bias for the STD (a-e) and MUMM (f-j) algorithms for moderately (m, $\rho_w(869) > 10^{-4}$ and $\rho_w(869) < 3.10^{-3}$) and very (v, $\rho_w(869) > 3.10^{-3}$)) turbid waters and when considering only the extremely turbid waters (e, $\rho_w(869) > 10^{-2}$). Box plots indicate median with first and third quartiles, upper and lower whiskers and outliers (small circles, $\pm 1.5IQR$). The horizontal grey lines indicate a bias of 0% (occurring when $\rho_w(\lambda)$ are perfectly retrieved).

3.2. Performances of the algorithms with the proposed modifications

In Figs. 3(a)-3(c) the performances of the initial and modified algorithms are compared. To evaluate the impact of imperfections in the retrieved η, Figs. 3(a)-3(c) also show the performances of the MUMM and polynomial-based MUMM algorithms when η is estimated for a

#193504 - $15.00 USD Received 8 Jul 2013; revised 12 Aug 2013; accepted 13 Aug 2013; published 3 Sep 2013

C90 aerosol model while the C50 aerosol model was used to simulate $\rho_{rc}(\lambda)$ (error on η of $\sim -40\%$). Table 1 shows the number of retrieved data and the median, mean and standard deviation of the percentage bias per wavelength when considering all retrieved reflectance spectra. Since the initial STD algorithm retrieves more spectra compared to the constrained algorithm, statistics are also given for the initial STD algorithm when only the spectra retrieved with the constrained STD algorithm are considered.

Table 1. Number of retrieved reflectance spectra and median (average, standard deviation) percentage bias per wavelength (412, 488, 547, 667, 748, and 869 nm). For comparison, statistics for the original STD algorithm are also given when considering only the spectra retrieved with the constrained STD algorithm.

	Numb. spectra	412	488	547	667	748	869
STD	95	-8 (-16, 40)	-4 (-5, 12)	-2 (-2, 6)	-2 (-4, 8)	-1 (-10, 28)	10 (-4, 40)
	90	-8 (-11, 29)	-4 (-4, 11)	-2 (-2, 5)	-2 (-5, 8)	-4 (-11, 28)	9 (-6, 40)
STD_{Con}	90	-4 (-2, 23)	-2 (-2, 10)	-1 (-1, 5)	-2 (-4, 8)	-6 (-13, 28)	-6 (-17, 34)
MUMM	105	-2 (-14, 54)	-1 (-7, 27)	-1 (-5, 17)	-2 (-5, 12)	-8 (-13, 21)	-13 (-17, 28)
$MUMM_{Poly}$	105	-1 (-8, 49)	0 (-4, 25)	0 (-3, 16)	-1 (-4, 12)	-2 (-11, 23)	-4 (-14, 30)

Overall the constrained STD algorithm shows improvements compared to the initial algorithm (lower median, mean and standard deviation). For moderately turbid waters, initial and constrained STD algorithms show similar results. Improvement with the constrained STD algorithm are more pronounced for very turbid waters and in particular in the blue and NIR region of the spectrum [Figs. 3(b) and 3(c)]. However, as shown in Table 1, the number of retrieved spectra is lower when the algorithm is constrained. Indeed, 15 spectra (all presenting extremely turbid water masses, $\rho_w(869) > 10^{-2}$) are excluded because the estimated Chl_a concentration was non-physical at least twice during the iterative process, while, with the initial STD algorithm, 9 spectra are excluded because the algorithm failed to retrieve Chl_a concentrations more than twice and 1 spectrum is excluded because the retrieved $\rho_w(667)$ did not converge within 10 iterations. For 13 spectra, out of the 15 spectra, $\rho_w(667)$ was corrected during the iterative process because it exceeded the maximum limit according to the red bounding spectral relationships suggested by Lee et al. [19]. When excluding this constrain (i.e., only retaining the NIR spectral relationship [18] in the NIR-modeling scheme), the number of excluded spectra decreases from 15 to 8. However, the performance of the algorithm decreases too, and in particular in the blue region of the spectrum over very turbid waters (not shown here). When considering only equivalent spectra, the STD algorithm constrained with both red and NIR spectral relationships slightly improves $\rho_w(\lambda)$ for all water types compared to the initial STD algorithm (Table 1). Hence, overall both the red and NIR spectral constrains improved the retrieved $\rho_w(\lambda)$ for all turbidity ranges. However, more work should be done to increase the number of retrieved spectra and thus reducing the sensitivity of the algorithm to non-physical Chl_a concentration estimations.

As expected from the validation exercise conducted by Goyens et al. [12], replacing the constant MUMM algorithm with the NIR polynomial relationship reduces the bias (Table 1) and mainly when considering only extremely turbid waters [Fig. 3(c)]. However, when including the NIR polynomial relationship, the algorithm seems to be more sensitive to errors on the estimated η. Hence, the added value of the polynomial NIR spectral relationship will be significantly reduced, when η is not correctly retrieved [Figs. 3(b)-3(c)]. Errors on the estimated η may be due to missing clear water pixels within the area of interest or if the assumption of spatial homogeneity in aerosol properties is not verified. This confirms the conclusion of Jamet et al. [7], notably that the sensitivity of the algorithm to the selected aerosol model remains an issue for the MUMM algorithm. Hence, compared to the MUMM algorithm, the STD algorithm presents a large advantage as it does not require an initial guess for η and does not

#193504 - $15.00 USD Received 8 Jul 2013; revised 12 Aug 2013; accepted 13 Aug 2013; published 3 Sep 2013

imposes spatial homogeneity in aerosol properties since it retrieves the aerosol properties on a pixel-by-pixel basis. However, as mentioned earlier, the STD algorithm is affected by erroneous Chl_a estimations. Moreover, relying only on a Chl_a based relationship to estimate $\rho_w(\lambda_{NIR})$ in optically complex waters may be dubious.

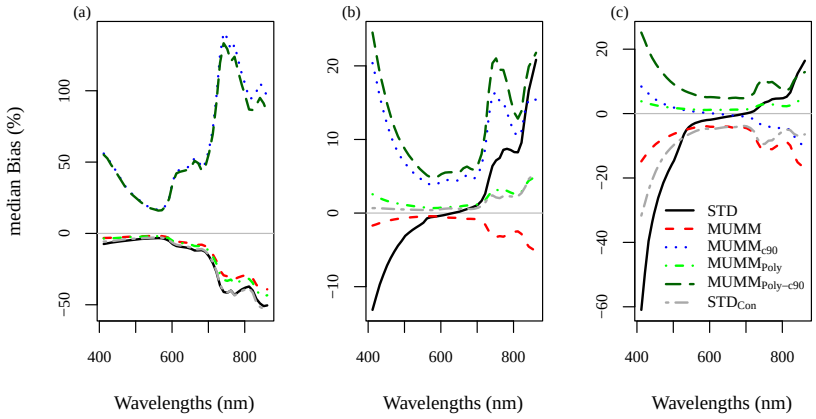

Fig. 3. Median percentage bias as a function of wavelength for (a) moderately and (b) very turbid waters and (c) when considering only the most turbid waters ($\rho_w(869) > 10^{-2}$) with STD: initial STD Algorithm, MUMM: initial MUMM algorithm assuming the correct aerosol model, MUMM$_{c90}$: MUMM algorithm assuming the incorrect C90 aerosol model, MUMM$_{Poly}$: polynomial-based MUMM algorithm, MUMM$_{Poly-c90}$: polynomial-based MUMM algorithm assuming the incorrect C90 aerosol model, and STD$_{Con}$: constrained STD algorithm.

4. Conclusion

More work needs to be done to further reduce inaccuracies in $\rho_w(\lambda)$ retrieved from ocean color images and particularly in turbid and optically complex waters [8]. Therefore, the present study aims to evaluate if $\rho_w(\lambda)$ retrievals can be improved by forcing the NIR-modeling scheme within the standard NASA and MUMM GW94-based AC algorithms (referred to as the STD and MUMM algorithms) with spectral relationships validated previously in a companion paper from Goyens et al. [12]. According to the authors, the red bounding relationships used in the QAA [19] as well as the NIR spectral relationship suggested to extent the GW94 AC algorithm for the AC of GOCI images [18], were valid for moderately turbid and very turbid waters. These relationships are used here to constrain the initial MUMM and STD algorithms. Two modified algorithms are evaluated: (1) a modified MUMM algorithm where the NIR constant $\rho_w(\lambda)$ ratio is replaced by the polynomial NIR spectral relationship, and (2) a modified STD algorithm where the iterative NIR-modeling scheme is constrained with the bounding red spectral relationships suggested by Lee et al. [19] and the NIR polynomial relationship [18] to evaluate $\rho_w(869)$ from $\rho_w(748)$. The degree of improvement resulting from the spectral relationship constrains are investigated by comparing *in situ* $\rho_w(\lambda)$ with $\rho_w(\lambda)$ retrieved with the initial and modified STD and MUMM algorithms.

When the STD algorithm is forced with the bounding red and the NIR polynomial spectral relationships, the algorithm performs better for all turbidity ranges and over the entire spectrum. However, the number of retrieved $\rho_w(\lambda)$ spectra is slightly reduced because more spectra are

#193504 - $15.00 USD Received 8 Jul 2013; revised 12 Aug 2013; accepted 13 Aug 2013; published 3 Sep 2013

flagged due to non-physical Chl_a concentration estimations in the NIR-modeling scheme.

When the constant NIR reflectance ratio used in the initial MUMM algorithm to account for non-zero $\rho_w(\lambda_{NIR})$, is replaced by the NIR polynomial relationship [18], errors in estimated $\rho_w(\lambda)$ are reduced, particularly in extremely turbid waters. However, compared to the initial algorithm, the polynomial-based MUMM algorithm is more sensitive to erroneously estimated η from nearby clear water pixels.

Compared to the MUMM algorithm, the STD algorithm presents a large advantage as it does not require an initial guess for η neither imposes spatial homogeneity in aerosol properties. Accordingly, the MUMM algorithm should be further improved to reduce the sensitivity of the algorithm to the selected aerosol model. Meanwhile, the STD algorithm should be modified such that $\rho_w(\lambda)$ retrievals are less affected by erroneous estimations of Chl_a concentrations. Accordingly, further improvements in $\rho_w(\lambda)$ retrievals may be achieved by, for instance, combining both polynomial-based MUMM and constrained STD algorithms. This may be investigated in a future research.

The present study investigates the feasibility to constrain NIR-modeling schemes with spectral relationships in the aim to improve AC processes and subsequently satellite estimated $\rho_w(\lambda)$. This study should be confirmed by an *in situ*-satellite data match-up exercise to verify and quantify the effective improvement in satellite $\rho_w(\lambda)$ retrievals resulting from the suggested modifications.

Acknowledgments

Most of the *in situ* measurements used here were collected in the framework of the BELCOLOUR-1 and BELCOLOUR-2 projects funded by the Belgian Science Policy Office STEREO programme. Griet Neukermans and Barbara Van Mol are acknowledged for data acquisition. This work has been supported by the French Spatial Agency (CNES) through the TOSCA program and the "Ministère de l'Enseignement et de la Recherche Française" which provided a PhD scholarship.

#193504 - $15.00 USD Received 8 Jul 2013; revised 12 Aug 2013; accepted 13 Aug 2013; published 3 Sep 2013